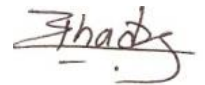


Declaration

I hereby declare that the work presented in this Thesis titled *Assessment of nonlinear responses and bifurcation analysis of light-weight shaft disk system with different loading configurations*, submitted to the Indian Institute of Technology Jodhpur in partial fulfilment of the requirements for the award of the degree of Doctor of Philosophy, is a bonafide record of the research work carried out under the supervision of Professor *Dr. Barun Pratiher*. The contents of this thesis in full or in parts, have not been submitted to, and will not be submitted by me to, any other Institute or University in India or abroad for the award of any degree or diploma.



Mr. Phadatare Hanmant Pandurang

(P14ME008)

Department of Mechanical Engineering

Indian Institute of Technology Jodhpur

India-342037



॥ त्वं ज्ञानमयो विज्ञानमयोऽसि ॥

Department of Mechanical Engineering
Indian Institute of Technology Jodhpur
India-342037

Certificate

It is certified that the work contained in this thesis entitled “**Assessment of nonlinear responses and bifurcation analysis of light-weight shaft disk system with different loading configurations**” submitted by **Mr. Phadatare Hanmant Pandurang** to the Indian Institute of Technology Jodhpur for the award of the degree of Philosophy has been carried out under my supervision in the Department of Mechanical Engineering, Indian Institute of Technology Jodhpur. This work has not been submitted elsewhere for the award of any other degree or diploma.

The thesis, in my opinion, has reached the standard fulfilling the requirements for the award of the degree of Doctor of Philosophy in accordance with the regulations of the Institute.

(Dr. Barun Pratiher)

Associate Professor

Department of Mechanical Engineering

Indian Institute of Technology Jodhpur

India-342037

Acknowledgements

I thank my Ph.D. thesis Supervisor, *Professor Barun Pratiher*, for introducing me to the area of technical writing and its nuances. It has been an honour to be his first Ph.D. student. In the process, I have learned many technical and non-technical aspects of professional work. I am grateful to him for his *help* and *patience* as well as for constantly reminding me to be perfect in the little things that I do each day. His guidance helped me in all the time of research and writing of this thesis. I could not have imagined having a better advisor and mentor for my Ph.D study. Also, I am indebted to the Members of the Doctoral Committee, *Prof. B Ravindra*, *Prof. Sandeep Yadav* and *Prof. VVS Chandramauli* for their encouragement, insightful comments, and their enthusiastic guidance during the research work.

My stay at the institute was a wonderful experience because of my friends, *Pravesh*, *Aniket*, *Shivam*, *Rohit*, *Ram-Mohan Dileep* and *Aditya* for all the liveliness they infused into the non-academic part of the days at IIT Jodhpur. I also thank M. Tech students *Vinay*, *Sankalp*, and *Balaram* for their valuable assistance in carrying out the research work.

I acknowledge and thank my family: especially my wife, for the patience and love with which they ushered on me, and for bearing with me even when I was not spending time with them, and my brothers and sister for supporting me throughout writing this thesis and my life in general. I pay respects to my *parents* for all their love, sacrifices and blessings. I don't imagine a life without their love and blessings. Thank you for showing faith in me and for giving me the liberty to choose what I desired. I consider myself the luckiest in the world to have such a supportive family, standing behind me with their love and support.

I thank MHRD India for financial support by providing scholarship aid in my Ph.D. research work duration.

I thank God for giving me the strength and patience to work through all these years so that today I can stand proud with my head held high.

Mr. Phadatare Hanmant Pandurang

(P14ME008)

Department of Mechanical Engineering

Indian Institute of Technology Jodhpur

India-342037

List of Figures

Figures	Content	Page No.
Fig. 1.1	A basic model of a rotating system	1
Fig. 1.2	Applications in electrical power generation plant	2
Fig. 1.3	Applications in transportation	2
Fig. 1.4	Applications in heavy industries	3
Fig. 1.5	Accidents of rotating machines	5
Fig. 3.1	a) A rotating system with a rigid bearing System b) Elastic deformation in transverse direction	28
Fig. 3.2	Euler angle rotation	29
Fig. 3.3	Kinematics of a beam	30
Fig. 3.4	Conceptual spring-damper equivalent model for the bearings	33
Fig. 3.5	Unbalance mass position	35
Fig. 3.6	A rotor bearing system under moving platform	40
Fig. 3.7	Effect of location of disk on both linear and nonlinear forward and backward natural frequencies	43
Fig. 3.8	Effect of mass of the disk on both linear and nonlinear forward and backward natural frequencies	44
Fig. 3.9	Effect of the shaft diameter on both linear and nonlinear forward and backward natural frequencies with disk	44
Fig. 3.10	Linear forward and backward natural frequencies using Euler and Timoshenko theory; $L=0.5m$	45
Fig. 3.11	Linear forward and backward natural frequencies using Euler and Timoshenko theory; $L=0.06m$	45
Fig. 3.12	Time history of the free vibration of v ($\rightarrow Y$) and w ($\rightarrow Z$) directions.	45
Fig. 3.13	Effect of external frequency (Ω_2) on the dynamic performances of the rotor-bearing system; $M_e=0.12 \text{ kg}$,	46
Fig. 3.14	Effect of external amplitude on the dynamic performances of the rotor-bearing system.	48
Fig. 3.15	Effect of initial conditions on the dynamic performances of the rotor-bearing system.	49
Fig. 3.16	Influence of external amplitude on the frequency response curves.	50
Fig. 3.17	Variation of location of the disk on the frequency response curves.	50
Fig. 3.18	Variation of mass of the disk on the frequency response curves.	51
Fig. 3.19	Variation of radius of shaft on the frequency response curves.	51
Fig. 3.20	(a) Time history and phase portrait at the points P_1, P_2, P_3 (Fig. 3.14) (b) Time history	52
Fig. 3.21	Time history and phase portrait at the point (Fig. 3.14) with initial point $0.001, 0.001$.	52
Fig. 3.20	Effect of Mass unbalance on the frequency response curves.	53

Fig.3.22	a) A shaft disk system subjected to axial load b) Equivalent linear and nonlinear spring-damper system; State of elastic deformation in transverse direction (y, z)	54
Fig. 3.24	Mode shapes: a) Flexible bearing: $\lambda_1 = 3.45$, $\lambda_2 = 5.34$, $\lambda_3 = 7.14$ b) Rigid bearing	57
Fig. 3.25	Campbell diagram: $l_d = l/4$, $R_d = 0.08$ m	57
Fig. 3.26	Frequency response plots if $\Omega_1 \approx 2\omega_1$ and $\Omega_2 \approx \omega_1$: $P_0=1 \times 10^3$ N, $P_1=5 \times 10^3$ N, $K_l=1 \times 10^5$ N/m.	58
Fig. 3.27	Frequency response plot if $\Omega_1 \approx 2\omega_1$: $P_0=1 \times 10^3$ N, $P_1=5 \times 10^3$ N	59
Fig. 3.28	Frequency response plot if $\Omega_1 \approx 2\omega_1$: $P_1=5 \times 10^3$ N	59
Fig. 3.29	Frequency response plot if $\Omega_1 \approx 2\omega_1$: $P_0=1 \times 10^3$ N, $P_1=5.0 \times 10^3$ N	59
Fig. 3.30	Frequency response plot if $\Omega_1 \approx 2\omega_1$: $P_0=1 \times 10^3$ N	59
Fig. 3.31	Frequency response plot if $\Omega_1 \approx 2\omega_1$: $P_1=1 \times 10^3$ N, $P_0=5 \times 10^3$ N	60
Fig. 3.32	Frequency response plot if $\Omega_1 \approx 2\omega_1$: $P_1=1 \times 10^3$ N, $P_0=5 \times 10^3$ N	60
Fig. 3.33	Frequency response plot if $\Omega_1 \approx 2\omega_1$: $P_1=1 \times 10^3$ N, $P_0=5 \times 10^3$ N	60
Fig. 3.34	Frequency response plot if $\Omega_1 \approx 2\omega_1$ and $\Omega_2 \approx \omega_1$: $P_0=1 \times 10^3$ N, $P_1=1 \times 10^3$ N	61
Fig. 3.35	Frequency response plot if $\Omega_1 \approx 2\omega_1$ and $\Omega_2 \approx \omega_1$: $P_0=1 \times 10^3$ N	61
Fig. 3.36	Frequency response plot if $\Omega_1 \approx 2\omega_1$ and $\Omega_2 \approx \omega_1$: $P_1=5 \times 10^3$ N	61
Fig. 3.37	Frequency response plot if $\Omega_1 \approx 2\omega_1$ and $\Omega_2 \approx \omega_1$: $P_0=1 \times 10^3$ N, $P_1=5 \times 10^3$ N	61
Fig. 3.38	Frequency response plot if $\Omega_1 \approx 2\omega_1$ and $\Omega_2 \approx \omega_1$: $P_0=1 \times 10^3$ N, $K_{nl}=1 \times 10^9$ N/m ³	62
Fig. 3.39	Frequency response plot if $\Omega_1 \approx 2\omega_1$ and $\Omega_2 \approx \omega_1$: $P_0=1 \times 10^3$ N, $K_l=1 \times 10^5$ N/m	62
Fig. 3.40	Frequency response plot: $\Omega_1 \approx 2\omega_1$	62
Fig. 3.41	Steady state response only (Ref. Fig. 3.38) a) Time response b) FFT plot c) Phase portrait and Poincare map	63
Fig. 3.42	Frequency response plot	63
Fig. 3.43	Steady state response only (Ref. Fig. 3.40) a) Time response b) FFT plot c) Phase portrait d) Poincare map	64
Fig. 3.44	a) Bifurcation diagram of P_1 b) Time response plot: $\Omega_1 = 0.8\omega_1$, $P_0= 5000$ N, $K_l=2 \times 10^5$ N/m, $K_{nl}=3 \times 10^9$ N/m ³	64
Fig. 3.45	Bifurcation diagram of P_1 , $P_0=5000$ N, $K_l=2 \times 10^5$ N/m, $K_{nl}=3 \times 10^9$ N/m ³	65
Fig. 3.46	Steady state response only a) Time response b) FFT plot c) Phase portrait: $P_1 = 15000$ N, $P_0=5000$ N, $K_l=2 \times 10^5$ N/m, $K_{nl}=3 \times 10^9$ N/m ³	65
Fig. 3.47	Validation-Frequency response plot	66
Fig. 4.1	Graphical representation of flexible rotor-bearing consisting rotating shaft with rigid disk	69
Fig. 4.2	Euler angles rotation	70
Fig. 4.3	Time history for rotating shaft without disk effect in Y direction (v) for $\Omega = 10$ Hz $M = 0$.	74
Fig. 4.4	Time history for rotating shaft without disk effect in Z direction (w) for $\Omega = 10$ Hz, $M = 0$	74
Fig. 4.5	Time history for rotating shaft without disk effect in Y direction (v) for $\Omega = 10$ Hz	75
Fig. 4.6	Time history for rotating shaft without disk effect in Z direction (w) for $\Omega = 10$ Hz	75
Fig. 4.7	Time history for rotating shaft with and without disk system in Y direction (v) for $\Omega = 10$ Hz, and $M = 1.5$.	75

Fig. 4.8	Time history for rotating shaft with and without disk system in Z direction (w) for $\Omega = 10$ Hz, and $M = 1.5$.	75
Fig. 4.9	Time history for rotor-bearing system in Y direction for $\Omega = 10$ Hz, $M = 1.5$ and $I_2 = 0.00625$	75
Fig. 4.10	Time history for rotor-bearing system in Z direction for $\Omega = 10$ Hz, $M = 1.5$ and $I_2 = 0.00625$	75
Fig. 4.11	Forward and backward natural frequencies of shaft element only.	76
Fig. 4.12	Forward and backward natural frequencies of shaft with disk element for $M = 1.5$ and $L_d = L/3$	76
Fig. 4.13	Effect of mass ratio (M) on forward and backward natural frequencies of shaft with disk system for $I_2 = 0.00625$	76
Fig. 4.14	Effect of disk location L_d on forward and backward natural frequencies of shaft with disk system for $M = 1.5$ and $I_2 = 0.00625$	76
Fig. 4.15	Forward and backward natural frequencies of shaft with and without disk $I_2 = 0.00625$	77
Fig. 4.16	Influence of mass of moment of inertia (I_2) on nonlinear forward and backward natural frequencies of rotor-bearing system $M = 1.5$.	77
Fig. 4.17	Influence of mass ratio (M) on nonlinear forward and backward natural frequencies of rotor-bearing system for $I_2 = 0.00625$ and $L_d = L/3$	77
Fig. 4.18	Effect of disk location (L_d) on nonlinear forward and backward natural frequencies of shaft with disk system; $M = 1.5$ and $I_2 = 0.00625$	77
Fig. 4.19	Nonlinear forward and backward natural frequencies for the system with and without disk for $I_2 = 0.00625$ and $L_d = L/3$.	78
Fig. 4.20	Frequency diagram to indicate the differences between linear and nonlinear forward and backward natural frequencies for $M = 1.5$, $I_2 = 0.00625$ and $L_d = L/3$	78
Fig. 4.21	Fourier spectrum at a spin speed ($\Omega = 0$) for $M = 1.5$, $I_2 = 0.00625$ and $L_d = L/3$	78
Fig. 4.22	Influence of rotary inertia on nonlinear forward and backward natural frequencies of rotor-bearing system for $I_2 = 0.0225$ and $L_d = L/3$.	78
Fig. 4.23	Fourier spectrum at a spin speed $\Omega = 20$ rad/s (a) Linear case (b) Nonlinear case	79
Fig. 4.24	Fourier spectrum at a spin speed $\Omega = 50$ rad/s (a) Linear case (b) Nonlinear case.	79
Fig. 4.25	Fourier spectrum at a spin speed $\Omega = 100$ rad/s (a) Linear case (b) Nonlinear case.	80
Fig. 4.26	Influences of initial conditions on the nonlinear Natural frequencies at a spin speed $\Omega = 50$ rad/s	80
Fig. 4.27	Time history and Poincare's section at a spin speed $\Omega = 0$ rad/s for $c = 0$.	81
Fig. 4.28	Time history and Poincare's section at a spin speed $\Omega = 0$ Hz for $c = 0.05$ Ns/m	81
Fig. 4.29	Time history and Poincare's section at a spin speed $\Omega = 10$ Hz for $c = 0.0$ Ns/m	81
Fig. 4.30	Time history and Poincare's section at a spin speed $\Omega = 10$ Hz for $c = 0.05$ Ns/m.	82
Fig. 4.31	Conceptual model for unbalance and eccentricity	82
Fig. 4.32	a) Campbell diagram b) FFT plot of initial 3sec data at $\Omega = 0$ Hz : $v(0) = 0.15$, $w(0) = 0.00$	85
Fig. 4.33	Frequency response plot	85
Fig. 4.34	Steady state response only (Ref. Fig. 4.33) .a) Time response b) Phase portrait c) Poincare map	86
Fig. 4.35	Frequency response curve for Different eccentricity ($e_v = e_w$).	86

Fig. 4.36	Frequency response curve for different disk position (L_d)	86
Fig. 4.37	Frequency response curve for different disk mass (β_1)	87
Fig. 4.38	Frequency response curve for different unbalance (β_2): $\beta_1=0.5$.	87
Fig. 4.39	Frequency response curve for different diametrical moment of inertia (I_3)	87
Fig. 4.40	Frequency response curve for the rotating system with and without disk (same unbalance magnitude ($\beta_2 e_{v1}$) for both cases)	87
Fig. 4.41	Steady state response only. a) Time response b) Phase portrait c) Poincare map. : $v(0) = 0.01$, $e_v = e_w, e_{v1} = e_{w1} = 0.2374$	88
Fig. 4.42	Steady state response only. a) Time response b) FFT plot c) Phase portrait d) Poincare map. : $v(0) = 0.01$, $e_v = e_w = 0.1880$, $e_{v1} = e_{w1} = 0.2374$	88
Fig. 4.43	Steady state response only. a) Time response b) FFT plot c) Phase portrait d) Poincare map. : $v(0) = 0.01$, $e_v = e_w = 0.2505$, $e_{v1} = e_{w1} = 0.30$	89
Fig. 4.44	Steady state response only. a) Time response b) Phase portrait c) Poincare map. : $e_v = e_w = 0.125$	90
Fig. 4.45	Steady state response only. a) Time response b) FFT plot c) Phase portrait d) Poincare map. : $e_v = e_w = 0.125$, $\Omega = 4.485$	90
Fig. 4.46	Steady state response only. a) Time response b) FFT plot c) Phase portrait d) Poincare map. : $e_v = e_w = 0.125$, $\Omega = 5.485$	91
Fig. 4.47	a) Time response b) FFT plot c) Poincare map. : $e_v = e_w = 0.125$, $\Omega = 5.685$	91
Fig. 4.48	Bifurcation diagram a) Spin speed (Ω) Vs Poincare points (v) with ($v(0) = 0.01$) b) eccentricity (e_v) Vs Poincare points (v) with ($v(0) = 0.01$, $\dot{v}(0) = 0.02$, $w(0) = 0.0001$, $\dot{w}(0) = 0.01$)	92
Fig. 4.49	Bifurcation diagram a) β_2 Vs Poincare points (v) b) β_2 Vs Poincare points (v) with ($v(0) = 0.001$), $\dot{v}(0) = 0$, $w(0) = 0$, $\dot{w}(0) = 0$, $e_v = e_w = 0.02$	92
Fig. 4.50	Steady state response only (Ref. Fig. 4.49). a) Time response b) Phase portrait c) Poincare map	92
Fig. 4.51	Steady state response only (Ref. Fig. 4.49). a) Time response b) Phase portrait c) Poincare map. $\beta_2 = 0.28$	93
Fig. 4.52	a) Mode shapes b) Frequency response curve: $K_l = 0.016$, $C_b = 8.57 \times 10^{-4}$	94
Fig. 4.53	Frequency response curve: $K_l = 0.016$, $C_b = 8.57 \times 10^{-4}$	94
Fig. 4.54	Bifurcation diagram a) K_{nl} Vs Poincare points (v) with ($v(0) = 0.001$), $\dot{v}(0) = 0$, $w(0) = 0$, $\dot{w}(0) = 0$, $\beta_2 = 0.018$, $e_v = e_w = 0.02$	94
Fig. 4.55	Steady state response only (Ref. Fig. 4.54). a) Time response b) Phase portrait c) Poincare map	94
Fig. 4.56	Steady state response only (Ref. Fig. 4.54) a) Time response b) Phase portrait c) Poincare' map $K_{nl} = 78$	95
Fig. 4.57	Validation: Frequency response plot	95
Fig. 4.58	Schematic diagram of rotating system with rub impact phenomenon	96
Fig. 4.59	Bifurcation Diagram: Effect of spin speed (Ω)	99
Fig. 4.60	Effect of spin speed a) Time series b) FFT c) Phase portrait map d) Poincare' map: $\Omega = 2.3$.	99
Fig. 4.61	Effect of spin speed a) Time series b) FFT c) Phase portrait map d) Poincare' map: $\Omega = 2.8$.	100
Fig. 4.62	Effect of spin speed a) Time series b) FFT c) Phase portrait map d) Poincare' map: $\Omega = 3$.	101
Fig. 4.63	Bifurcation Diagram: Effect of unbalance mass (M_e)	101
Fig. 4.64	Effect of unbalance mass a) Time series b) FFT c) Phase portrait map d) Poincare' map: $M_e = 0.02$.	102

Fig. 4.65	Effect of unbalance mass a) Time series b) FFT c) Phase portrait map d) Poincare' map: $M_e = 0.08$.	103
Fig. 4.66	Effect of unbalance mass a) Time series b) FFT c) Phase portrait map d) Poincare' map: $M_e = 0.175$.	104
Fig. 4.67	Bifurcation diagram: Effect of coefficient of Friction (η)	104
Fig. 4.68	Effect of coefficient of Friction a) Time series b) FFT c) Phase portrait map d) Poincare' map: $\eta = 0.01$.	105
Fig. 4.69	Effect of coefficient of Friction a) Time series b) FFT c) Phase portrait map d) Poincare' map: $\eta = 0.15$.	105
Fig. 4.70	Bifurcation Diagram: Effect of stiffness of rub surface (i.e. stator) $1/K_r$	106
Fig. 4.71	Effect of stiffness of rub surface a) Time series b) FFT c) Phase portrait map d) Poincare' map: $1/K_r = 0.0167$.	107
Fig. 4.72	Effect of stiffness of rub surface a) Time series b) FFT c) Phase portrait map d) Poincare' map: $1/K_r = 3.34$.	107
Fig. 4.73	Effect of stiffness of rub surface a) Time series b) FFT c) Phase portrait map d) Poincare' map: $1/K_r = 2.67 \times 10^3$.	108
Fig. 5.1	A rotating system model with multiple disks	111
Fig. 5.2	Frequency response curve for multiple disks	116
Fig. 5.3	Frequency response curve for different loss factor (δ)	116
Fig. 5.4	Frequency response curve for different magnitude of the base excitation (W_b)	117
Fig. 5.5	Frequency response curve	117
Fig. 5.6	a) Time series b) Phase portrait map c) Poincare' map (Ref. Fig. 5.5)	118
Fig. 5.7	Bifurcation diagram for effect of δ , $N=4$, $\Omega_b = 50$,	118
Fig. 5.8	Bifurcation diagram for effect of δ , $N=2$, $\Omega_b = 72$,	118
Fig. 5.9	Effect of loss factor δ a) Time series b) Phase portrait map c) Poincare' map	119
Fig. 5.10	Bifurcation diagram for effect of W_b , $N=4$, $\Omega_b = 50$	119
Fig. 5.11	Bifurcation diagram for effect of W_b , $N=2$, $\Omega_b = 72$	119
Fig. 5.12	Effect of W_b a) Time series b) Phase portrait map c) Poincare' map	120
Fig. 5.13	Effect of W_b a) Time series b) Phase portrait map c) Poincare' map ($W_b = 0.05$)	120
Fig. 5.14	Bifurcation diagram for effect of Ω_b , $N=4$	120
Fig. 5.15	Bifurcation diagram for effect of Ω_b , $N=2$	120
Fig. 5.16	Effect of Ω_b a) Time series b) Phase portrait map c) Poincare' map	121
Fig. 5.17	Effect of Ω_b a) Time series b) Phase portrait map c) Poincare' map ($\Omega_b = 50$)	121
Fig. A.1	Displacement relation and Euler angle	141

List of Tables

TABLE 3.1: PARAMETERS OF A ROTATING MODEL

56

List of Symbols

Symbols	Descriptions
A	Cross sectional area of the Shaft in m^2
c	Viscous Damping coefficient of the shaft Ns/m
c_b	Damping coefficient of bearing in Ns/m
E	Modulus of elasticity N/m^2
e	Strain along shaft axis in m
e_v	Eccentricity of the shaft in y direction in m
e_w	Eccentricity of the shaft in z direction in m
F_x	Rubbing force in Y direction
f_x	Non dimensional Rubbing force in Y direction
F_y	Rubbing force in Y direction
f_y	Non dimensional Rubbing force in Y direction
h	Thickness if the disk in m
I_1	Polar mass moment of inertia $kg-m^2$
I_2	Diametrical mass moment of inertia $kg-m^2$
I_A	Area moment of inertia in mm^4
K_l	Linear stiffness coefficient of a bearings in N/m
K_{nl}	Nonlinear bearing stiffness coefficient in N/m^3
K_r	Stiffness of rub surface
L	Length of the shaft in m
L_d	Disk location from one of the ends of the shaft in m
m	Mass of the shaft in kg
M	Mass of the disk in kg
m_u	Unbalance Mass in kg
N	Number of discs
N_b	Linear forward natural frequency
N_{bn}	Non-linear forward natural frequency
N_f	Linear forward natural frequency
N_{fn}	Non-linear forward natural frequency
P_0	Static axial force in N
P_1	Pulsating axial force in N
r_1	Eccentricity of the unbalance mass in m
R_d	Radius of the disk in m
R_s	Radius of the shaft in m
u, v, w	Displacements in x, y and z directions
Z_a, W_b	Amplitude of base excitation
ψ, θ and β	Angular displacement about the axes of Z, Y, and X
θ_1	Non dimensional disk mass

β_2	Non dimensional unbalance mass
δ	Loss Factor or Clearance between rotor and stator
Δx	Eccentricity of stator axis with rotor in Y direction
Δy	Eccentricity of stator axis with rotor in Z direction
η	Coefficient of friction
λ	Eigen value of mode shape function
ρ	Mass Density of the shaft in kg/m^3
σ	Detuning parameter
Ω	Rotating speed/ Excitation frequency in rad/s
Ω_1	Frequency of an axial force excitation in rad/s
ω_1	Forward Natural frequency in rad/s
Ω_2	Spinning speed of the rotor in rad/s
ω_2	Backward Natural frequency in rad/s
ω_e, Ω_b	Base excitation frequency

List of Abbreviations

<i>Abbreviation</i>	<i>Full form</i>
<i>BNF</i>	Backward Natural Frequency
<i>BNNF</i>	Backward Nonlinear Frequency
<i>DOF</i>	Degree of Freedom
<i>FFT</i>	Fast Fourier Transform
<i>FNF</i>	Forward Natural Frequency
<i>FNNF</i>	Forward Nonlinear Natural Frequency
<i>HBM</i>	Harmonic Balance Method
<i>MI</i>	Moment of inertia
<i>MMS</i>	Method of Multiple Scales
<i>NNM</i>	Nonlinear Normal Mode
<i>Ph.D.</i>	Doctor of Philosophy
<i>S-N</i>	Saddle Node

